ORIGINAL ARTICLE

A study on berthing and unberthing of a single-shaft ship with a bow thruster

R. Okuda[1] · H. Yasukawa[2] · N. Hirata[1] · A. Matsuda[3]

Abstract

In this study, the berthing and unberthing performances of a single-propeller and single-rudder inland container ship with a flapped rudder and bow thruster were investigated using free-running model tests. A navigation method was used for the tests to adjust the bow thruster, so that the heading remained parallel to the pier and the ship berths or unberths while sailing in oblique conditions. As a result, the proposed method enables the target ship to berth or unberth in shallow water with $h/d = 1.5$, where h is the water depth and d is the ship draft. Such a free-running test using the navigation method is useful for evaluating the berthing and unberthing performance of single-shaft ships with a bow thruster. In addition, a bow thruster impeller revolution controller was incorporated into the maneuvering simulation model proposed by the authors, and berthing calculations were performed. The calculation results were compared with free-running test results for validation. These results are consistent with the free-running test results with practical accuracy.

Keywords Berthing · Unberthing · Single-shaft ship · Flap rudder · Bow thruster · Shallow water effect

1 Introduction

When a ship is berthing or unberthing, collisions with the quay walls or other ships are most likely to occur. Therefore, safe navigation is essential. Attempts have been made to improve ship safety using automatic navigation technology for berthing and unberthing. Kose et al. [1] indicated a two-step process to achieve automatic berthing: first, route planning (navigation plan) and then guidance based on it (maneuvering control). For example, a berthing simulation has been conducted for a ship assisted by multiple tugs. Koyama et al. [2] and Yamato et al. [3] discussed automatic berthing for single-shaft ships with bow and stern thrusters. Wu et al. [4] also discussed automatic berthing for a single-shaft ship with bow and stern thrusters. However, the target

ships for these studies could potentially be crabs that use various maneuvering devices.

In principle, single-propeller and single-rudder ships without bow and stern thrusters cannot move laterally, because the propeller induces forward motion. Therefore, berthing and unberthing of single-shaft ships become more difficult. Hasegawa and Kidera [5], Maki et al. [6], and Sawada et al. [7] discussed automatic berthing for single-shaft ships. The simulation results for automatic berthing indicated that even a single-shaft ship could safely berth. However, the navigation method obtained involves frequent normal and reverse rotations of the propeller and is difficult to apply directly to an actual ship.

In this study, we used free-running model tests to examine the berthing and unberthing performance of a single-propeller and single-rudder inland container ship with a bow thruster. Here, a navigation method was used to adjust the bow thruster, so that the ship heading remained parallel to the quay and the ship berths and unberths while sailing obliquely. This method is called the 'oblique sailing navigation (OSN)' method. After confirming that berthing and unberthing are possible by free-running model tests using the OSN-method, the influence of the rudder type, such as the difference between the flap rudder and normal rudder; the influence of the rudder angle; and the influence of water

✉ H. Yasukawa
  yasukawa@hiroshima-u.ac.jp

1 Hiroshima University, Higashihiroshima, Japan

2 Graduate School of Advanced Science and Engineering, Hiroshima University, Kagamiyama 1-4-1, Higashihiroshima, Hiroshima 739-8527, Japan

3 Japan Fisheries Research and Education Academy, Kamisu, Japan

Table 1 Principal particulars of the subject ship (Suzaku)

	Full-scale	Model
L [m]	83.0	3.000
B [m]	13.5	0.488
d [m]	3.8	0.1376
∇ [m³]	3146	0.1486
C_b	0.737	
x_G [m]	0.930	0.034
$\overline{GM}$ [m]	0.91	0.0329
D_P [m]	2.80	0.101
p	0.694	
Z	5	

depth on the berthing and unberthing performance were investigated experimentally. These investigations demonstrated that the berthing and unberthing performances of single-propeller and single-rudder ships could be evaluated. In addition, we incorporated a bow thruster impeller revolution control model to simulate the OSN-method in the low-speed maneuvering model proposed by Okuda et al. [8] and calculated the berthing motion. The calculation results were compared with free-running test results for validation.

2 Studied ship

The studied ship is an inland container ship called "Suzaku" [9], that navigates coastal areas in Japan. The ship is a 749GT container carrier with the capacity of 204TEU, and a single-propeller and single-rudder ship with a bow thruster.

2.1 Hull, propeller and bow thruster

Table 1 lists the principal particulars of the full-scale ship and its model. In the table, L denotes the length between the perpendiculars. B is the breadth, d is the draft, ∇ is the displacement volume, C_b is the block coefficient, x_G is the longitudinal coordinate of the center of gravity, $\overline{GM}$ is the metacentric height, D_P is the propeller diameter, p is the propeller pitch ratio, and Z is the number of propeller blades. The scale ratio of the model was 1/27.667. Figure 1 shows a photo of the ship model. The bilge keels attached to the model were fitted between S.S.3.15 and 6.76. The length of the bilge keel model was 1084.3 mm, and the protruding height was 23.5 mm.

A 4-blade bow thruster (BT) model with a diameter (D_B) of 55.0 mm (1.52 m on the full-scale ship) was attached to the ship model at S.S.9.43. The longitudinal distance of the BT position from the midship is 0.443L. Figure 2 shows a photo of the BT model.

2.2 Flapped rudder

The ship is equipped with a flap rudder, as shown in Fig. 3. The flap rudder provides a higher rudder force than conventional rudders, because the flap assumes a certain angle with the rudder. A large lift force is expected from the flap effect. Figure 4 shows profile and rudder cross-sectional shape of the flapped rudder model used in the tank tests. Table 2 lists the dimensions of the rudder. H_R denotes the rudder span length, B_R is the chord length, including the flap part, and A_R is the total rudder profile area. H_R was determined as A_R/B_R. The chord length of the main rudder
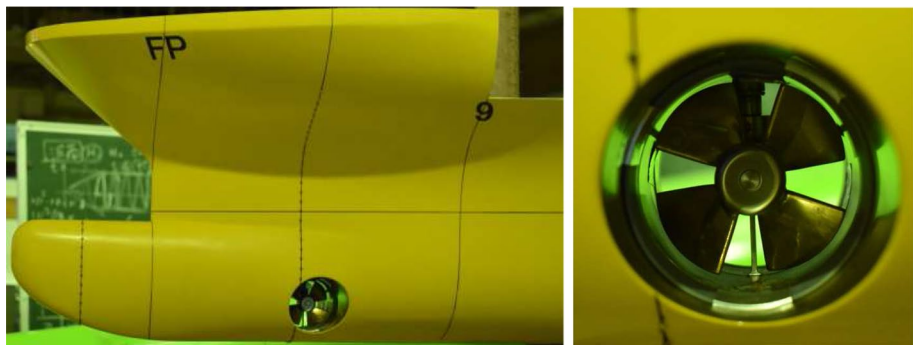

Fig. 1 Ship model of the subject ship (Suzaku)

Fig. 2 Bow thruster model
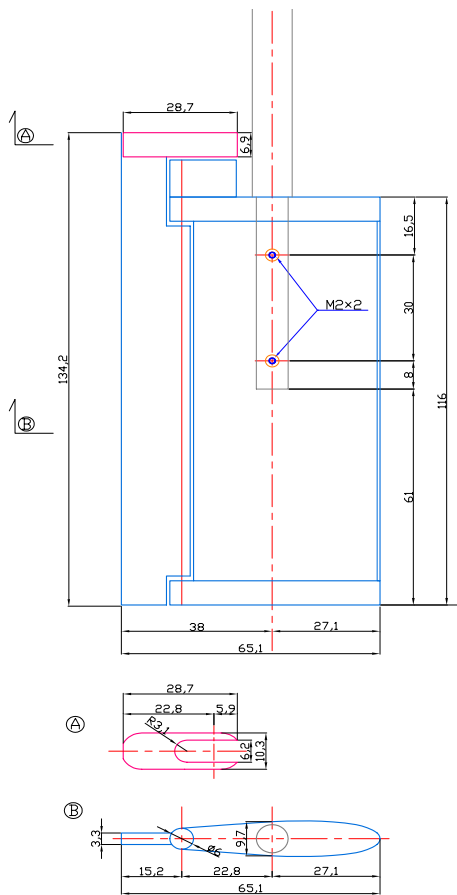
Fig. 3 Flap rudder model

Fig. 4 Profile and rudder cross-sectional shape of a flapped rudder model

Fig. 5 Slide-link mechanism for a flapped rudder

Table 2 Principal particulars of rudder

	Full-scale	Model
H_R [m]	3.43	0.124
B_R [m]	1.80	0.065
A_R [m^2]	6.180	0.00807

was 0.050 m, and that of the flap was 0.015 m. The flap area was approximately 23% of the total rudder area.

The main rudder and flap part of the rudder model were connected by a slide-link mechanism similar to that of a full-scale ship, as shown in Fig. 5. In the figure, P is rudder shaft center and R is flap shaft center. The position R changes with the rudder angle δ. A position Q is fixed to the ship hull and Q is pin-connected to an upper-plate of the flap part. The flap part moves with the upper-plate. The Q can move along a groove dug between Q and R for a slide-link mechanism (actually, Q is fixed to the hull, so the upper-plate with the groove moves). With such the mechanism, the flap angle δ_F can be automatically obtained with an ordered rudder angle δ. The δ_F value versus δ is determined by PQ and PR distances. For the target ship, δ_F value changes, as shown in Fig. 6.
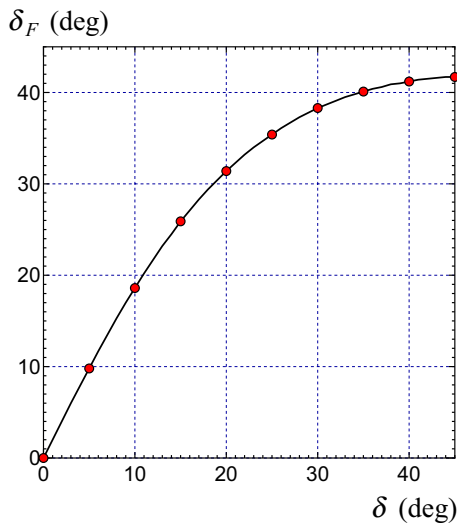
Fig. 6 Flap angle (δ_F) versus rudder angle (δ)

Table 3 Condition of water depth, h

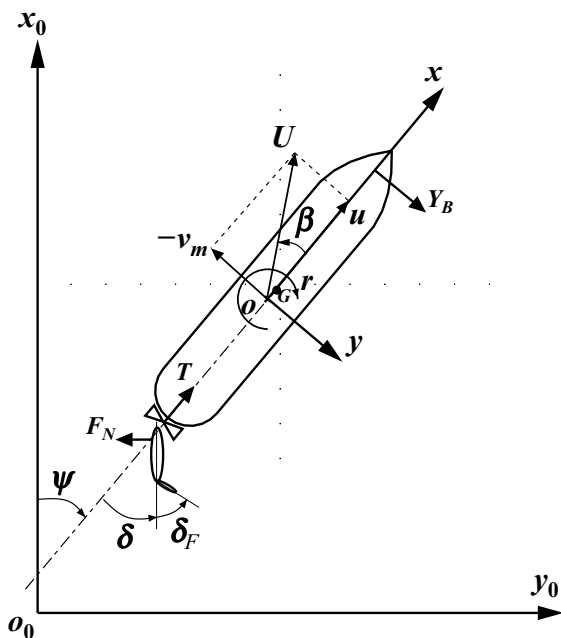| h/d	Full-scale [m]	Model [m]
23.3 (deep)	88.5	3.2
1.5	5.70	0.206
1.2	4.56	0.165

3 Free-running model tests for berthing

and unberthing

3.1 Coordinate systems

Figure 7 shows the coordinate systems used herein. In the ship-fixed coordinate system $o - xyz$, where o is taken at midship, u and v_m denote the velocity components in the x and y directions, respectively. In contrast, we consider a space-fixed coordinate system, where the $x_0 - y_0$ plane coincides with the still water surface and the z_0-axis points vertically downward. The center of gravity G is located at position $(x_G, 0)$. x_G is the longitudinal coordinate of the center of gravity (forward from the midship is positive). The angle generated from x_0 to x is defined as heading angle ψ. r is the yaw rate around the z-axis, as defined by $d\psi/dt$. The hull drift angle at the midship position β is defined as $\beta = \tan^{-1}(-v_m/u)$ and the total velocity U is defined as $U = \sqrt{u^2 + v_m^2}$. Moreover, δ is the rudder angle, and δ_F is the flap angle. F_N is the rudder normal force and T is the propeller thrust. Y_B denotes the lateral force generated by the bow thruster.

Figure 8 shows the space-fixed coordinate system when berthing and unberthing tests in shallow water. We consider the origin o_0 of the space-fixed coordinates at the edge of the pier, as shown in Fig. 8. We consider the x_0-axis along the longitudinal direction of the pier and the y_0-axis in the lateral direction.
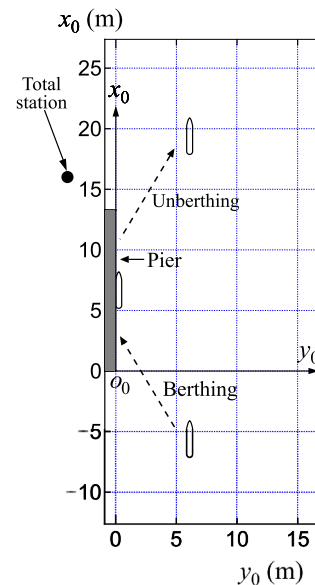

Fig. 7 Coordinate systems

Fig. 8 Space-fixed coordinate system when berthing and unberthing tests in shallow water

Table 4 Measurement items in free-running model tests

Equipment	Item
Total station	Position of ship model (x_0, y_0)
Fiber-optics gyroscope (FOG)	Heading (ψ), yaw rate (r), roll (ϕ)
Propeller dynamometer	Propeller thrusts (T)
Rudder dynamometer	Rudder normal forces (F_N)
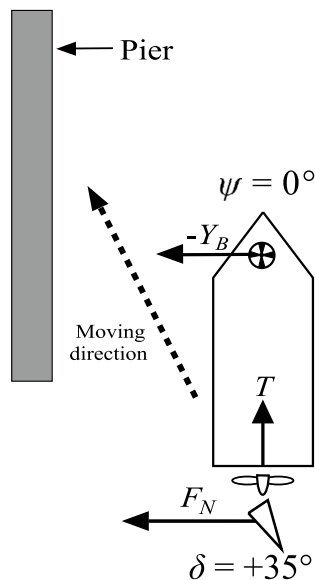
Fig. 9 Schematic diagram for berthing navigation

3.2 Overview of free-running model tests

Free-running model tests for berthing and unberthing were conducted in two basins of Japan Fisheries Research and Education Agency: Marine Dynamic Basin (tank length: 60 m; width: 25 m; depth: 3.2 m) for deep water tests, and Coastal Wave Test Basin (tank length: 40 m; width: 30 m; depth: 0.8 m (max)) for shallow water tests. For the berthing and unberthing tests conducted in shallow water, a pier model was placed in a Coastal Wave Test Basin. The pier model has a vertical wall between 0 m and 13.3 m in the longitudinal direction of the basin, as shown in Fig. 8. The length of the pier model is equivalent to 368 m in the full-scale pier. The tests were performed under three different water depth conditions: deep water and shallow water with $h/d = 1.5$ and 1.2, where h is the water depth, and d is the ship draft. Table 3 lists the water depths. In deep water, the free-running tests were conducted without the pier model.

The model conditions for the tests were as follows.

- The propeller revolution was set as 5.8 rps, which is equivalent to 4 kn in deep water (0.391 m/s in the ship

model). In shallow water, the tests were performed with the same propeller revolution.
- The steering rate was set as 12.2°/s (equivalent to 2.32°/s for full-scale).
- The maximum BT force was set to 3.04 N (equivalent to 6.5 tons for full-scale) for both port and starboard sides. The impeller revolution at that time was 37.0 rps for the starboard side thrust and 32.6 rps for the port side thrust.
- The radius of pitch gyration (k_{yy}) was set as $0.25L$.

Table 4 summarizes the measurement parameters and equipment used in the free-running model tests. The position of the ship model was measured using a Total Station system (TS) on land [10–12], which automatically tracked the target (Prizm) set in the ship model. Figure 8 shows the installation position of a theodolite for TS in the tank tests. The heading and yaw rates were measured using a fiber-optic gyroscope (FOG) installed on the ship model. The synchronization was performed using the same receiver (same received signal) for measurements on board and using the TS. The ship model was operated using a radio controller (T14SG, Futaba corporation). The measured data were wirelessly transmitted to a land-based computer. The ship's speed U and drift angle β are calculated by post-processing based on the measured position and heading data.

3.3 A navigation method for berthing and unberthing: OSN-method

The navigation methods for berthing and unberthing in the free-running tests were as follows:

1. When moving laterally to the port side, the rudder is set, as shown in Fig. 9. The rudder angle (δ) is constant at the specified value (+35°). At the same time, the BT is operated to generate lateral force (Y_B) directed to the port side. The BT impeller revolution is manually adjusted, so that the ship heading is kept parallel to the pier $(\psi = 0°)$. Note that the signs of the rudder angle and the BT impeller revolution are reversed when moving laterally to the starboard side.
2. The propeller revolution is fixed at the specified value (5.8 rps). The propeller thrust T is generated at that time, and the ship model moves forward gradually. A single-propeller and single-rudder ship, such as the target ship, cannot stop the forward movement without a change in the propeller revolution.
3. The BT impeller revolution is manually adjusted to keep the ship heading parallel to the pier $(\psi = 0°)$. In the case of berthing, as shown in Fig. 9, the ship model gradually approaches the pier while forward moving. Just before the ship model collides with the pier, the test ends. In the

case of unberthing, the test ends when the ship model is sufficiently far from the pier.

This method is called the 'oblique sailing navigation method' (OSN-method) in this paper. In the free-running tests for berthing and unberthing, measurements were started from the rest condition of the ship.

Because of the manual operation for the BT, the free-running test result changes depending on the proficiency of the operator. In the tests, after practicing several times, measurements were repeated 2 or 3 times, and the smoothest maneuvering result was employed as the test result in this paper.

3.4 Results of free-running tests for berthing and unberthing

The results of the free-running model tests are presented below. The basic test conditions were as follows:

- Equipped with a flapped rudder.
- The rudder angle; $\delta = \pm 35°$.
- The water depth; $h/d = 1.5$.

3.4.1 Effect of flapped rudder

To capture the effect of the flapped rudder on the berthing and unberthing performances, free-running tests were conducted using two rudders: a flapped rudder (FLAP) and a zero-flapped rudder (zeroF). At zeroF, the rudder shape was the same as that of FLAP. However, the flap angle was fixed at zero. ZeroF can be regarded as a normal rudder. Figure 10 shows a comparison of ship trajectories between FLAP and zeroF while berthing and unberthing. The shadows were plotted at the ship positions every 10 s from the start of the test. A significant difference was observed between FLAP and zeroF in the berthing and unberthing motions. Compared to zeroF, FLAP moves laterally with less forward movement.

To determine the lateral motion of a ship quantitatively, the lateral distance y_s is defined as follows:

$$y_s(t) = |y_0(t) - y_0(0)| \tag{1}$$

where y_0 represents the y_0-coordinates of the ship's trajectory as a function of time t. Figure 11 shows a comparison of time histories of the non-dimensional lateral distance y_s/L. y_s/L of FLAP is larger than that of zeroF, indicating that FLAP moves faster laterally. Specifically, y_s/L at $t = 60$ s for FLAP was larger approximately $0.2L$ when berthing,
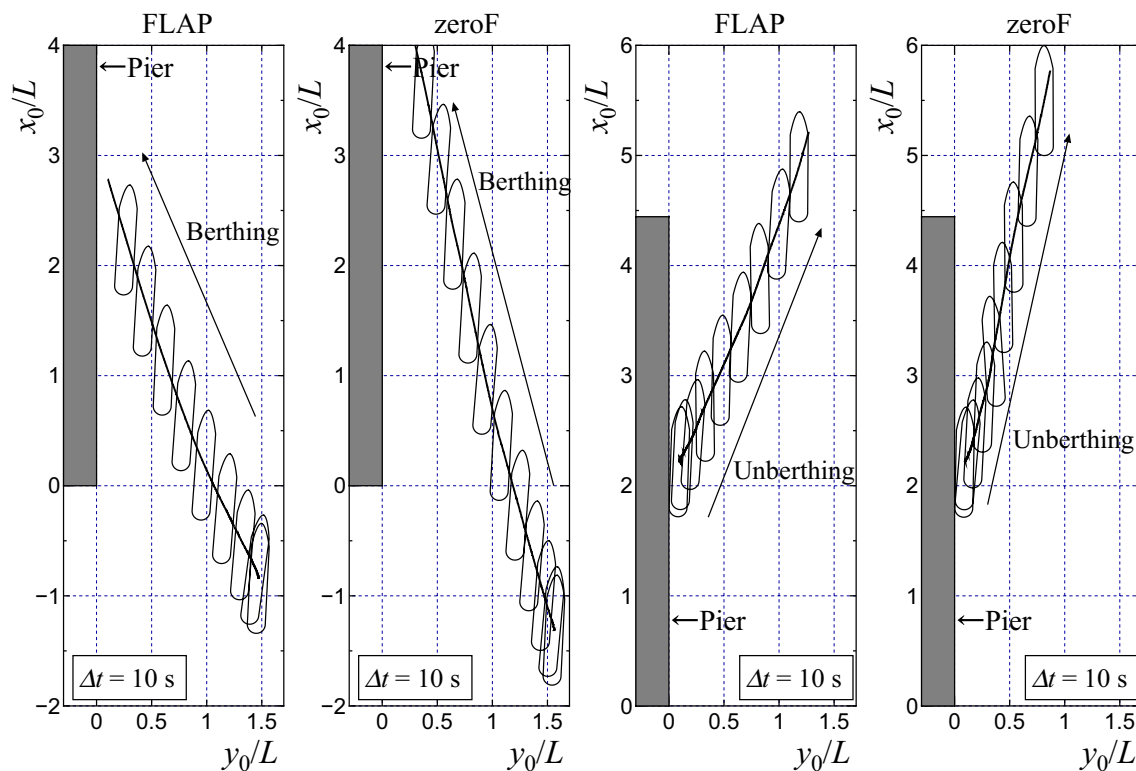

Fig. 10 Comparison of ship trajectories between FLAP and zeroF while berthing and unberthing in $h/d = 1.5$
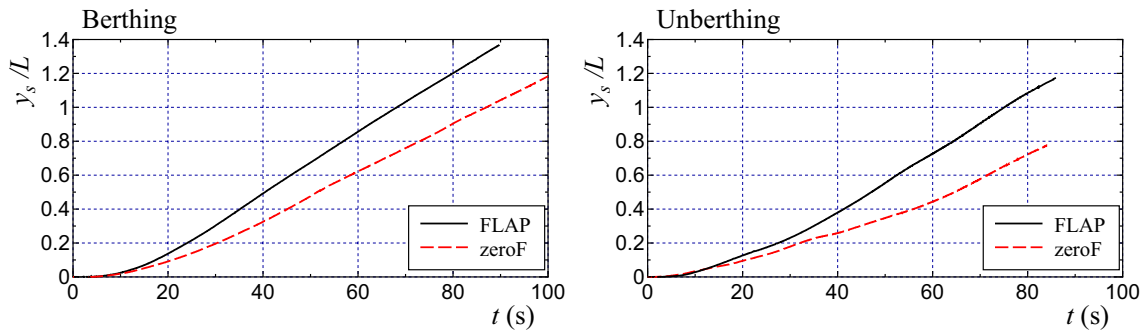
Fig. 11 Comparison of time histories of non-dimensional lateral distance y_s/L for FLAP and zeroF in $h/d = 1.5$

and 0.3L when unberthing than that for zeroF. The use of a flapped rudder increases the lateral speed. Thus, a flapped rudder is more effective than a normal rudder for berthing and unberthing. y_s/L during berthing was larger than that during unberthing for both FLAP and zeroF as a whole.

This implies that the lateral moving speed during berthing was higher.

Figure 12 compares time histories of drift angle β, normal rudder force F_N, and BT impeller revolution n_B for FLAP and zeroF. The absolute value of β for FLAP was larger than that for zeroF in both berthing and unberthing. Comparing
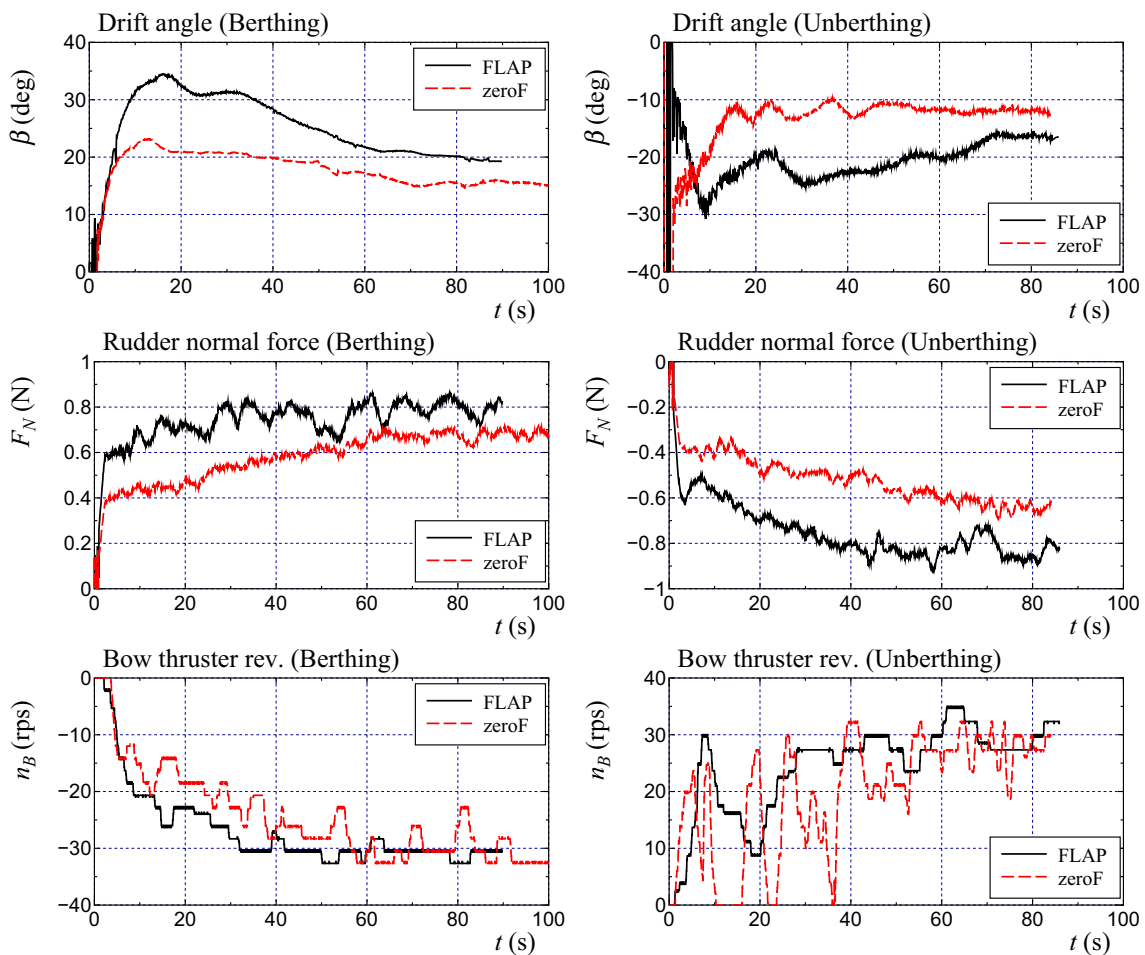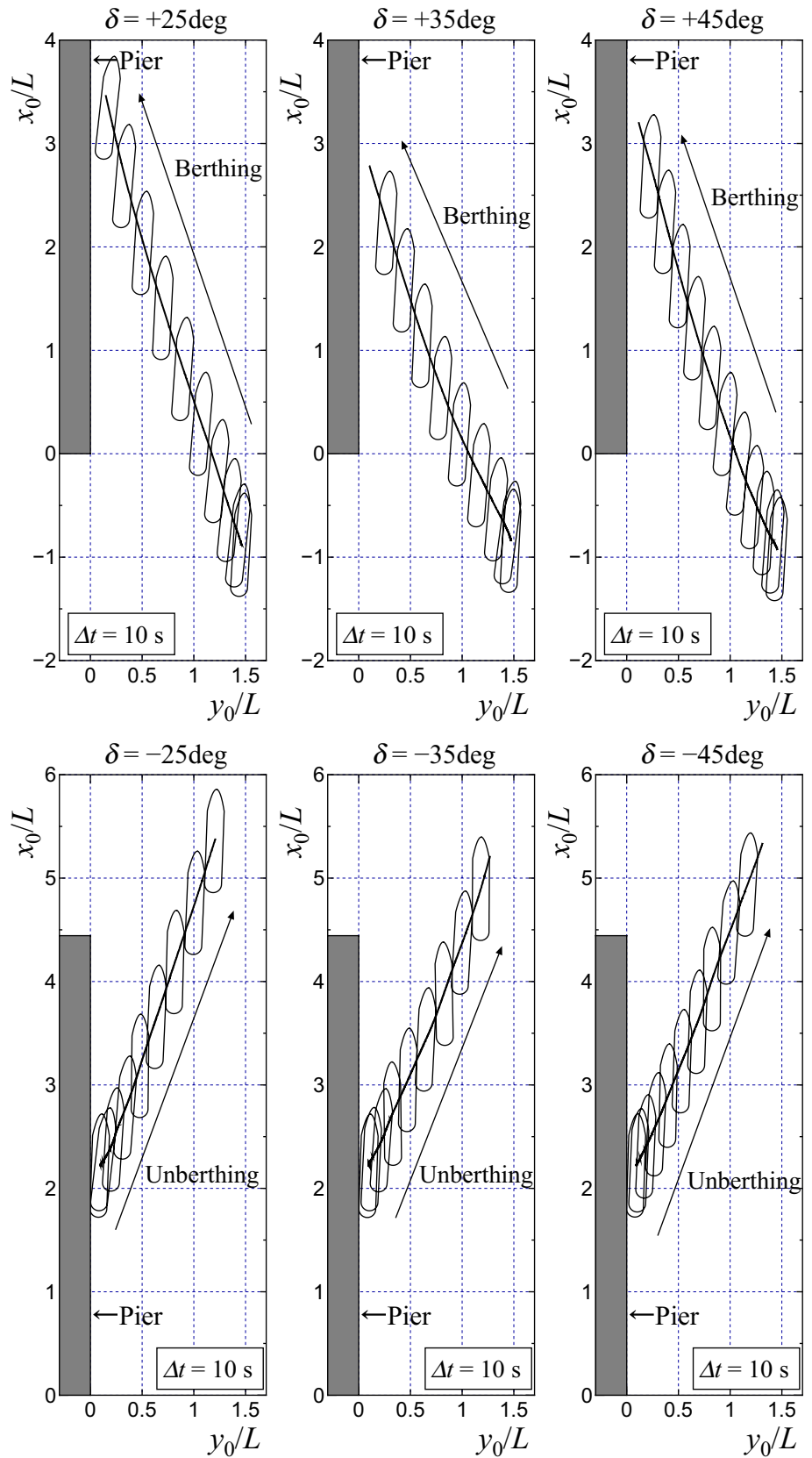

Fig. 12 Comparison of time histories of drift angle β, rudder normal force F_N, and BT impeller revolution n_B for FLAP and zeroF in $h/d = 1.5$ (left: berthing, right: unberthing)

Fig. 13 Comparison of ship trajectories while berthing and unberthing for different rudder angles in $h/d = 1.5$
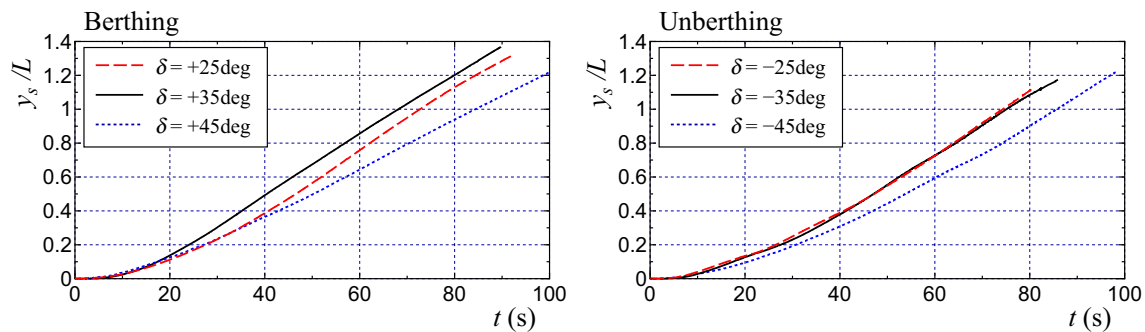
Fig. 14 Comparison of time histories of lateral distance y_s/L while berthing and unberthing for different rudder angles in $h/d = 1.5$

the absolute values of β at 60 s, FLAP is larger than zeroF by approximately 5° during berthing and approximately 9° during unberthing. The berthing and unberthing performances of FLAP are superior to those of zeroF. This is owing to the larger absolute value of the rudder normal force for FLAP than for zeroF, as shown in the time history of F_N. The absolute value of n_B for FLAP in berthing is larger than that for zeroF until $t = 60$ s. Because n_B is determined, such that the rudder force balances the generated BT thrust, the absolute value of n_B for FLAP with a larger F_N becomes larger than that for zeroF. However, when sufficient time passes, n_B for FLAP becomes almost the same as that for zeroF.

3.4.2 Effect of rudder angle

To determine the optimum rudder angle for berthing navigation, free-running tests were conducted at rudder angles of +25° and +45° in addition to the rudder angle +35°. Similarly, for unberthing navigation, the rudder angles are changed to −25°, −35°, and −45°. Figure 13 compares ship trajectories while berthing and unberthing for different rudder angles. There were no significant differences among the three trajectories for berthing and unberthing. Specifically, the ship's forward position (x_0/L) just before berthing at $\delta = +35°$ was approximately $0.5L$ behind at $\delta = +45°$, and approximately $1L$ behind at $\delta = +25°$. The forward movement during berthing is the smallest at $\delta = +35°$ and the forward movement the largest at $\delta = +25°$. Similarly, the forward movement during unberthing was the smallest at $\delta = −35°$ and the forward movement was the largest at $\delta = −25°$.

Figure 14 compares time histories of the lateral distance y_s/L. The y_s/L value for berthing was largest at $\delta = +35°$ and decreased in the order of $\delta = +25°$ and $\delta = +45°$. The y_s/L values for unberthing were almost the same at $\delta = −25°$ and $\delta = −35°$. Only y_s/L at $\delta = −45°$ was smaller.

Figure 15 shows comparison of time histories of β, F_N, n_B, and ship speed U during berthing and unberthing. In

berthing, β is the largest at $\delta = +35°$ from $t = 18$s to approximately $t = 60$s after the start of the lateral movement and is smaller in the order of $\delta = +45°$ and $\delta = +25°$. Subsequently, the three β values were approximately the same. β at unberthing is similar to the sign of the time-history result at berthing, except for the beginning of the lateral movement. F_N at berthing behaves roughly the same regardless of the rudder angle. However, after $t = 50$s, F_N is the smallest at $\delta = +45°$. F_N at unberthing also reverses the sign of the time history result at berthing. After $t = 50$s, because the absolute value of F_N is the smallest at $\delta = \pm45°$, in balance with the rudder force, the BT thrust required to maintain the ship heading is small. Therefore, the absolute value of n_B at $\delta = \pm45°$ is slightly lower than that of the others. For both berthing and unberthing, U increased with time and approached a constant value. The order of magnitude of U decreased with an increase in the absolute value of δ.

In general, increasing the rudder angle increases the rudder force and facilitates the lateral movement of the ship. However, if the rudder angle is excessively large, the berthing/unberthing performance deteriorates. To investigate the reason for this, a captive model test (rudder force test in straight motion) was conducted, in which the hydrodynamic forces acting on the ship model were measured by changing the rudder angle. Figure 16 shows the measured results of the surge force X and the lateral force Y versus the rudder angle δ. The tests were conducted under a model-propellered condition of $U = 0.587$ m/s with $n_P = 10.0$ rps at $h/d = 1.5$. X increases in the negative direction with an increase in the absolute value of δ, indicating that the ship resistance increases. The absolute value of Y increases with the absolute value of δ and becomes largest at $\delta = \pm25°$. If the absolute value of δ increases further, then the absolute value of Y decreases. In particular, at $\delta = +45°$, the absolute value of Y is approximately 30% smaller than that at $\delta = +25°$. This was probably owing to a stall occurring in the flap rudder.

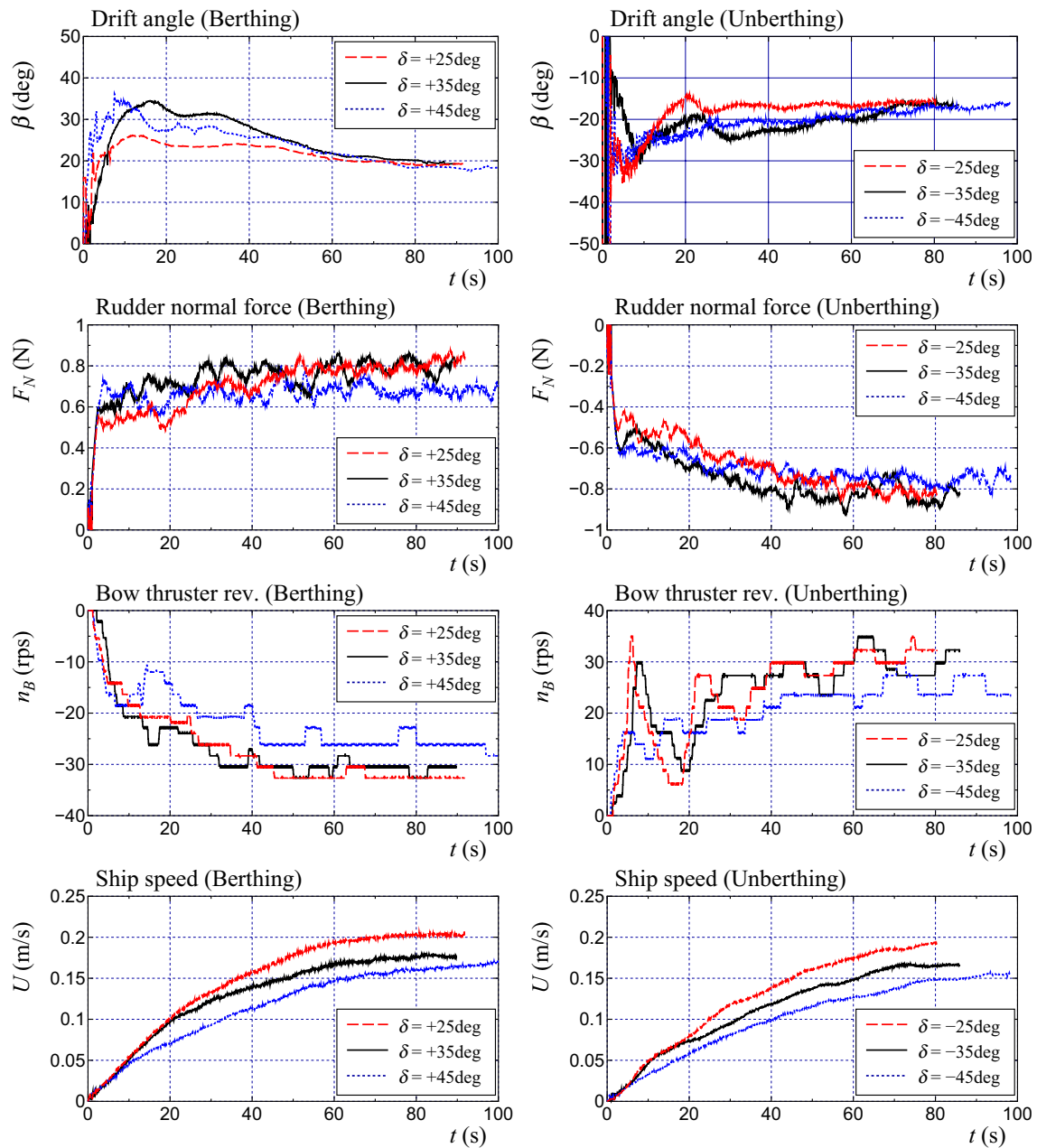**Fig. 15** Comparison of time histories of drift angle β, rudder normal force F_N, BT impeller revolution n_B, and ship speed U for different rudder angles (left: berthing, right: unberthing)

We know that there are two desirable ways to achieve better berthing and unberthing performances. One is to increase the lateral force Y, and the other is to increase the ship resistance by increasing X in the negative direction to suppress the forward movement. From these two perspectives, we compared the absolute values of X and Y for the three rudder angles +25°, +35°, and +45°. When $\delta = +25°$, the value of Y was the largest, whereas that of X was the smallest (ship resistance was the smallest). Therefore, it is difficult to suppress forward movement efficiently, and a larger lateral

force cannot be fully utilized. Conversely, when $\delta = +45°$, the value of X was the highest, whereas that of Y was the lowest. It is slightly easier to suppress the forward movement, but the lateral force is too small for efficient berthing or unberthing. When $\delta = +35°$, the balance between the suppression of the forward movement and the strength of the lateral movement is optimal, and efficient berthing and unberthing are possible.
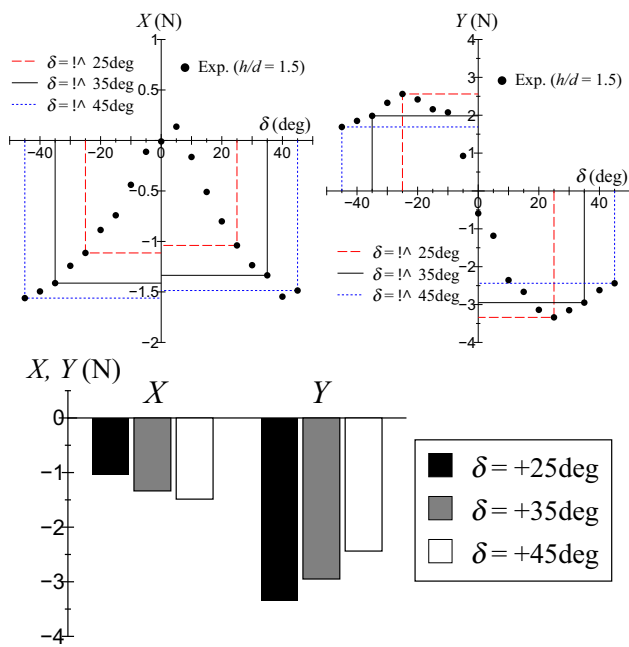
Fig. 16 Comparison of surge force X and lateral force Y acting on ship model in rudder force tests ($h/d = 1.5$)

3.4.3 Effect of water depth

Figure 17 compares ship trajectories while berthing and unberthing in $h/d = 1.2$ and lateral movement in deep water, in addition to $h/d = 1.5$. In deep water, the ship can move laterally with less forward movement than other ships. At $h/d = 1.5$, the ship can berth and unberth while maintaining a constant heading angle, although the forward movement is more significant than that in deep water. At $h/d = 1.2$, when approaching the pier, the ship cannot maintain a constant heading and turns around to move away from the pier. Hence, the ship cannot berth. In contrast, unberthing is possible, although lateral movement speed is slow. Figure 18 compares time histories of y_s/L for three different water depths. As the water depth becomes shallow, y_s/L decreases overall for both berthing and unberthing, and the speed of the lateral movement (or berthing and unberthing) decreases. Thus, the effect of water depth was significant for both berthing and unberthing. As the water depth becomes shallow, the forward movement of the ship becomes more remarkable, and lateral movement becomes difficult.

We now consider why the ship cannot berth when $h/d = 1.2$. The ship speed U gradually increases during berthing, as shown in Fig. 19. With an increasing ship speed, the hydrodynamic force acting on the ship hull increases, and the BT thrust required to maintain the heading also increases. In particular, for $h/d = 1.2$, the required BT thrust exceeded its maximum value because of the larger lateral

force on the ship hull (see Fig. 20), and the ship model reached an uncontrollable situation.

Figure 19 shows comparison of time histories of β, F_N, n_B, and U for three different water depths. The absolute value of β increases with increasing water depth for both berthing and unberthing and exceeds 40° after $t = 40$s in deep water. F_N exhibited a similar tendency for deep water, and $h/d = 1.5$. However, only the absolute value of F_N at $h/d = 1.2$ was smaller than those at the other water depths. There was no significant difference in the behavior of n_B even at different water depths. U at berthing exhibits similar behavior at any water depth. U at unberthing is slightly larger only in deep water and is almost the same for $h/d = 1.5$ and $h/d = 1.2$.

4 Berthing simulations

Next, maneuvering simulations of the berthing motion were conducted for the present ship using the mathematical model at large drift angles presented by Okuda et al. [8]. The simulation results are compared for validation with the berthing free-running test results described in the previous section. The simulation method was originally intended for ship maneuvering in the open sea and excluded the bank effect on the hydrodynamic forces of the ship during berthing. For the simulations, the radius of yaw gyration (k_{zz}) was assumed to be $0.25L$.

4.1 Hydrodynamic parameters used for simulations

4.1.1 Hydrodynamic parameters

Table 5 lists the hydrodynamic parameters used in these simulations. Most hydrodynamic parameters are determined using captive model tests [13]. The parameters used in deep water were the same as those presented by Okuda et al. [8]. The added mass and moment of inertia coefficients (m'_x, m'_y, and J'_{zz}) were obtained via calculations using the three-dimensional panel method [14]. The parameters related to the effective propeller thrust (t_P, w_{P0}, C_0) during maneuvering were obtained through oblique towing and circular motion tests. The hull-rudder interaction coefficients (t_R, a_H, x'_H) and parameters of the rudder normal force (ε and κ) were obtained through rudder force tests. The flow-straightening coefficients (γ_{R+}, γ_{R-}) were obtained through flow-straightening tests. Here, γ_{R+} is the coefficient for starboard turning, and γ_{R-} is for port turning. l'_R was determined based on the experimental results obtained by Yoshimura and Sakurai [15].

Fig. 17 Comparison of ship trajectories while berthing and unberthing or lateral movement for three different water depths
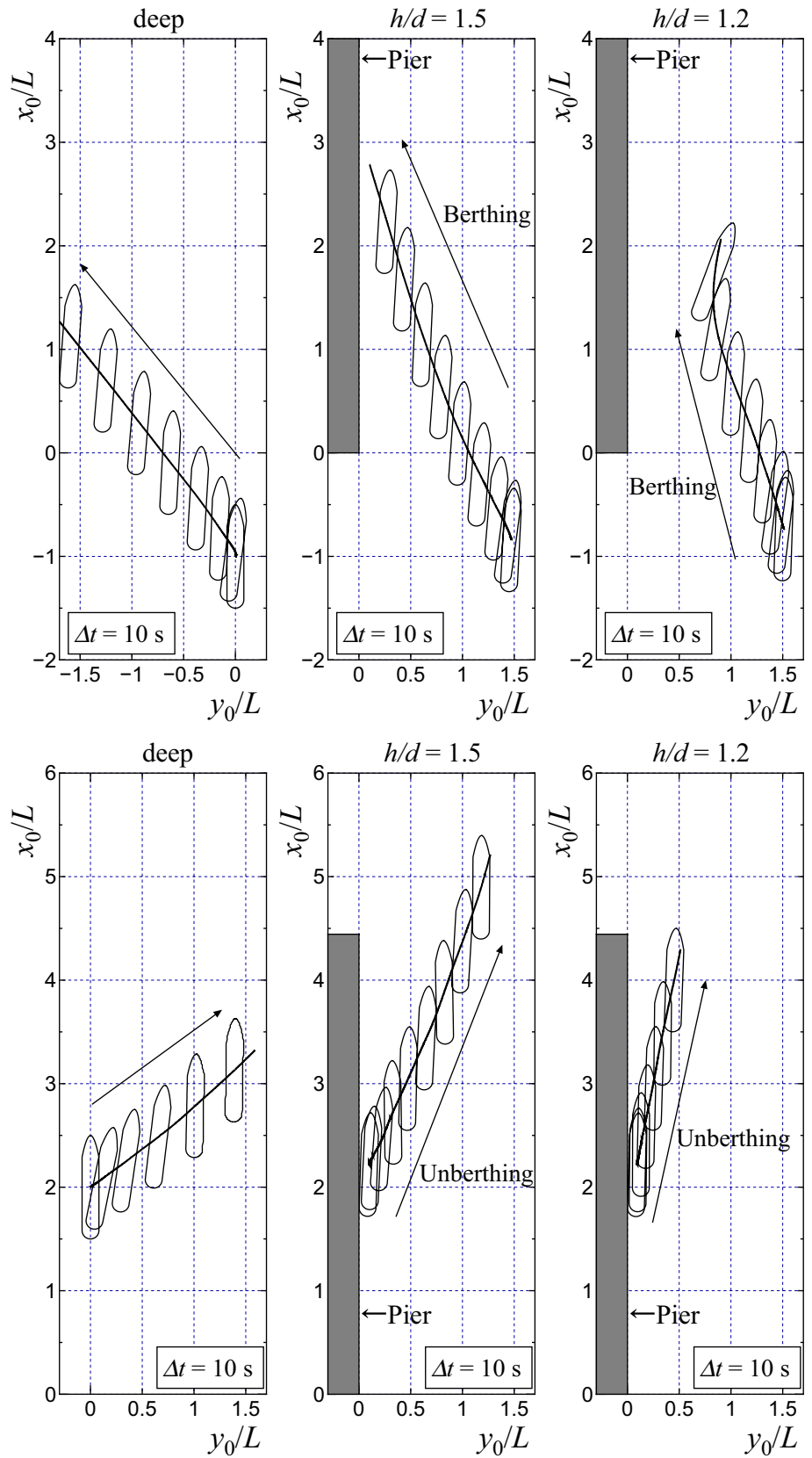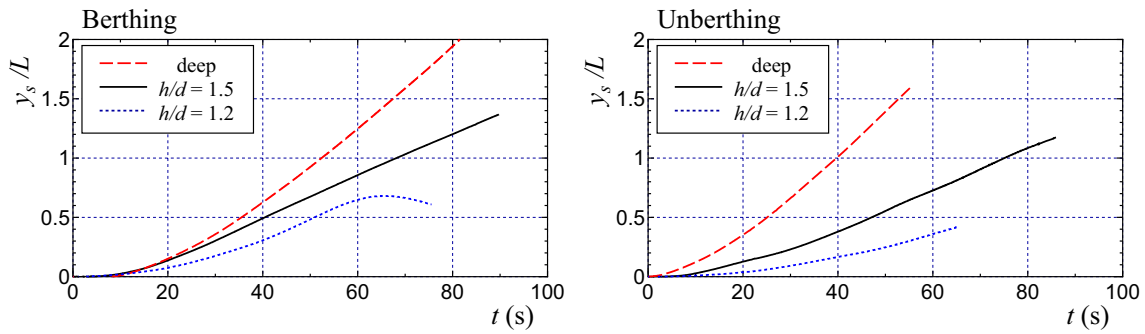
Fig. 18 Comparison of time histories of lateral distance y_s/L for three different water depths

4.1.2 Hull forces

The Table-model presented by Okuda et al. [8] was used as the hull hydrodynamic force model. The Table-model interpolates the hydrodynamic force characteristics based on a hydrodynamic force database organized by motion parameters, such as the drift angle β and yaw rate angle $\alpha_r (\equiv \tan^{-1}(rL/U))$. Figure 20 shows the hydrodynamic force database for surge force coefficient C_{HX}, lateral force coefficient C_{HY}, and yaw moment coefficient C_{HN} in three different water depths, such as deep water, $h/d = 1.5$, and $h/d = 1.2$. The forces and moment are nondimensionalized by $(\rho/2)Ld[U^2 + (Lr)^2]$ and $(\rho/2)L^2d[U^2 + (Lr)^2]$, respectively. These do not include the inertial force and added mass components. Furthermore, C_{HX} exclude the resistance component in straight moving. These results were obtained from captive model tests.

4.1.3 Hydrodynamic forces generated by bow thruster

The characteristics of the hydrodynamic force acting on the ship hull generated by the BT were calculated using the following procedure [8]:

1. Obtain the lateral force Y_{B0} and yaw moment N_{B0} acting on the ship model at rest.
2. Provide f_X, f_Y, and f_N representing the forward speed effect on the hydrodynamic forces generated by the BT
3. Calculate the hydrodynamic forces generated by the BT (X_B, Y_B, N_B) using the following formulas:

$$\left. \begin{array}{l} X_B = Y_{B0}(n_B)f_X(F_n) \\ Y_B = Y_{B0}(n_B)f_Y(F_n) \\ N_B = N_{B0}(n_B)f_N(F_n) \end{array} \right\} \tag{2}$$

where n_B is the BT impeller revolution and F_n the Froude number based on L. Note that Y_{B0} and N_{B0} are assumed to be constant with respect to lateral motion of the ship.

Figure 21 shows the lateral force Y_{B0} and yaw moment N_{B0} acting on the ship hull generated by the BT at rest in three different water depths. Y_{B0} and N_{B0} did not change significantly with the water depth. The tests results show an asymmetry that the absolute values of Y_{B0} and N_{B0} are different depending on the positive and negative of the n_B. This is caused by the asymmetric installation of the BT impeller device. Figure 22 shows the coefficients f_X, f_Y, and f_N versus F_n in three different water depths. The f_X, f_Y, and f_N represent the rates of change of X_B/Y_{B0}, Y_B/Y_{B0}, and N_B/N_{B0} by ship speed U, respectively. When $U = 0(F_n = 0)$, f_X is 0 and f_Y and f_N are 1. These were determined from captive model tests under BT working conditions with varying U. With an increase in F_n, f_X increases in the negative direction, and f_Y and f_N decrease.

4.2 A bow thruster impeller control model

Berthing calculations require a control model for BT thrust to simulate the OSN-method. In this study, PD control with feedforward correction was used to provide the optimal BT thrust. Specifically, the BT impeller revolution n_B is given by

$$n_B = n_{B0} - \psi G_{PB} - r G_{DB} \tag{3}$$

where G_{PB} is the proportional gain with respect to heading ψ and G_{DB} is the derivative gain of ψ (i.e., yaw rate r). n_{B0} is the estimated BT impeller revolution required to maintain heading ψ at zero. To maintain ψ at zero, the total yaw moment acting on the ship must be zero. Here, the following relational equation holds:

$$N_H + N_R + N_B = 0 \tag{4}$$

Here, N_H is the yaw moment acting on the ship hull, N_R is the yaw moment by steering, and N_B is the yaw moment
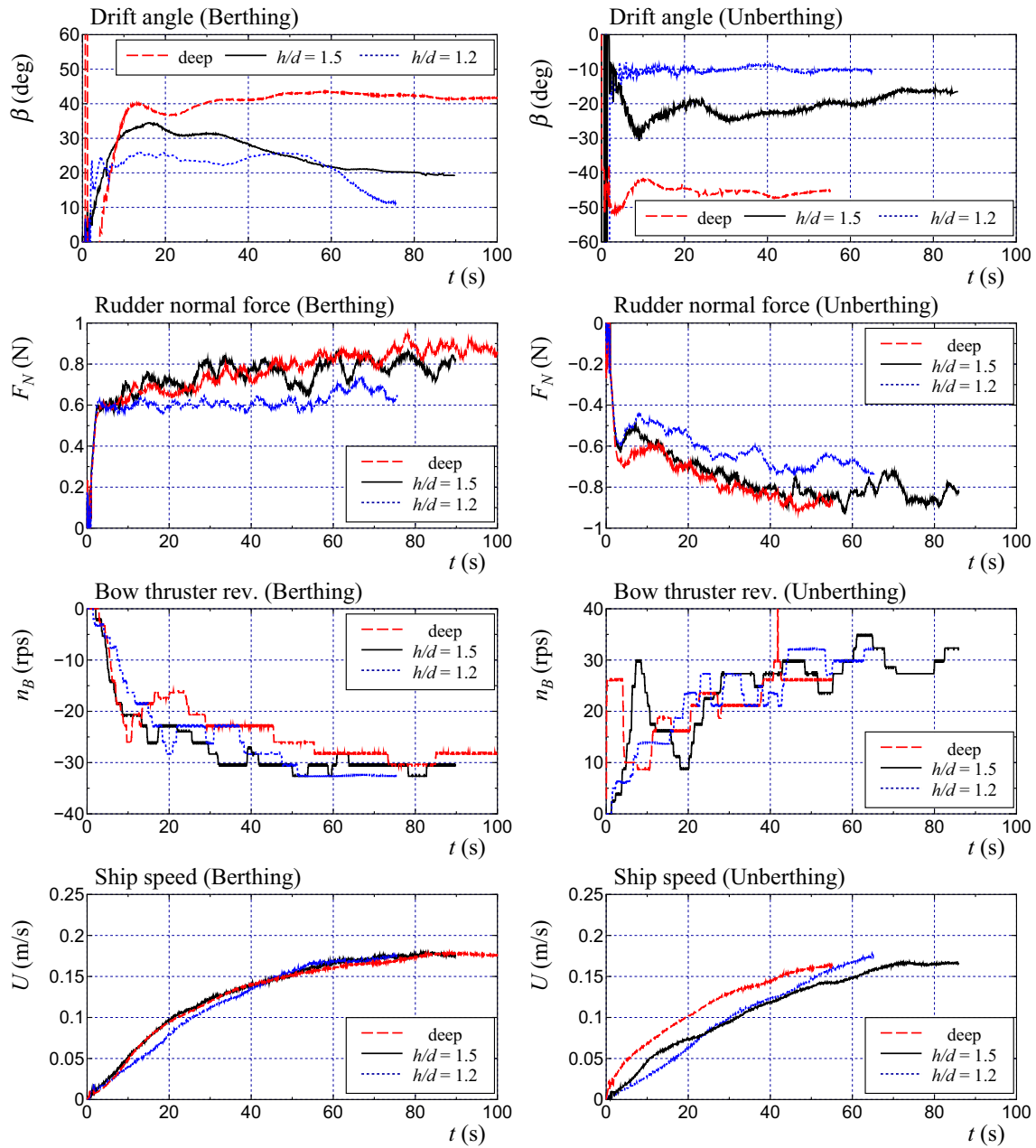
Fig. 19 Time histories of drift angle β, rudder normal force F_N, BT impeller revolution n_B, and ship speed U for three different water depths (left: berthing, right: unberthing)

owing to the BT. Therefore, N_B was determined using the following equation:

$$N_B = -(N_H + N_R) \tag{5}$$

In the berthing simulations, N_H and N_R can be estimated easily [8]. Thus, N_B is known. N_B is expressed as

$$N_B = \rho n_{B0}^2 D_B^4 L_B K_{NB} \tag{6}$$

where D_B is the impeller diameter, L_B is the longitudinal coordinate of the BT position, K_{NB} is the BT thrust coefficient, and n_{B0} is calculated as follows:

Table 5 Hydrodynamic parameters used in the maneuvering simulation

	Deep	$h/d = 1.5$		$h/d = 1.2$
	FLAP	FLAP	zeroF	FLAP
m_x'	0.010	0.027		0.034
m_y'	0.168	0.330		0.542
J_{zz}'	0.010	0.008		0.013
t_P	0.080	0.115		0.206
w_{P0}	0.422	0.710		0.850
C_0	−2.0	−4.0		−8.0
t_R	−0.058	−0.126	0.231	0.036
a_H	0.158	0.257	0.251	0.317
x_H'	−0.605	−0.436	−0.415	−0.410
ε	1.27	1.26		1.28
κ	0.50	0.55		0.53
γ_{R+}	0.483	0.713		0.566
γ_{R-}	0.308	0.470		0.449
l_R'	−0.888	−0.598		−0.518

$$n_{B0} = \text{sgn}(N_B)\sqrt{\frac{|N_B|}{\rho D_B^4 L_B K_{NB}}} \tag{7}$$

Table 6 lists the values of K_{NB} used in these simulations. K_{NB} is obtained using the captive model test, and we observed that K_{NB} is larger when $n_B < 0$ than when $n_B > 0$. Furthermore, K_{NB} decreased slightly as the water depth decreased.

In the simulations, the control gains were set to $G_{PB} = 1$ rps/deg and $G_{DB} = 1$ rps/(deg/s). Moreover, if the absolute value of n_B exceeds 37.0 rps when generating the thrust on the starboard side and 32.6 rps when generating the thrust on the port side, a limiter was provided to force the impeller revolution set to that value.

4.3 Lateral moving simulations in deep water

Maneuvering simulations of lateral movement in deep water were conducted. A flapped rudder was used in the simulation. Figure 23 compares ship trajectories while lateral moving with $\delta = \pm35°$ in deep water. In this case, there were

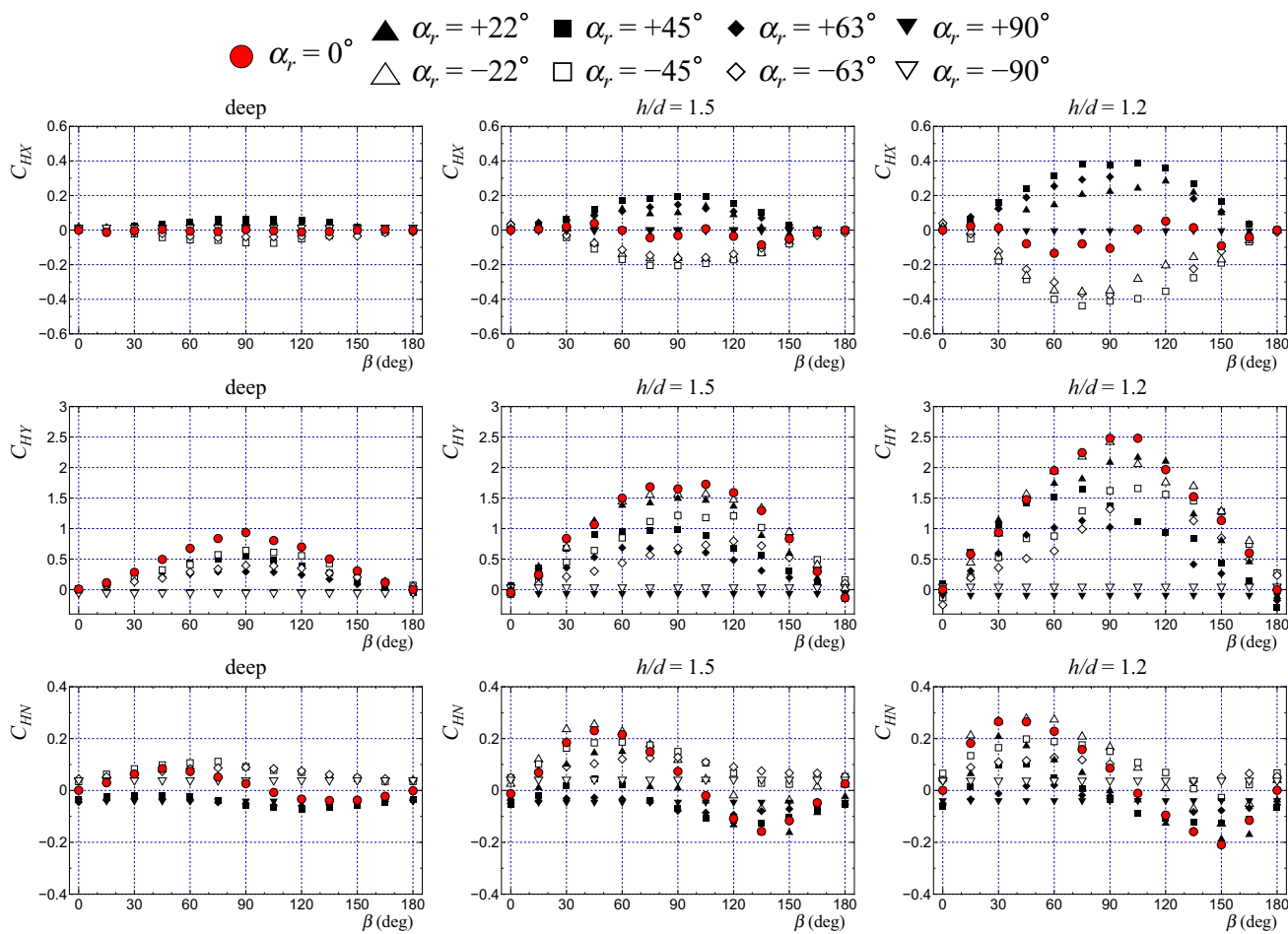**Fig. 20** Surge force coefficient C_{HX}, lateral force coefficient C_{HY}, and yaw moment coefficient C_{HN} in three different water depths

Fig. 21 Lateral force Y_{B0} and yaw moment N_{B0} generated by BT at $U = 0$ in three different water depths
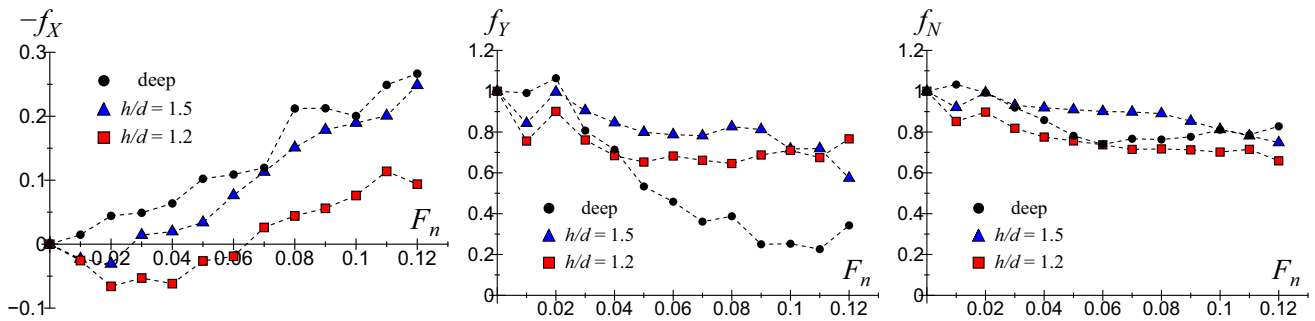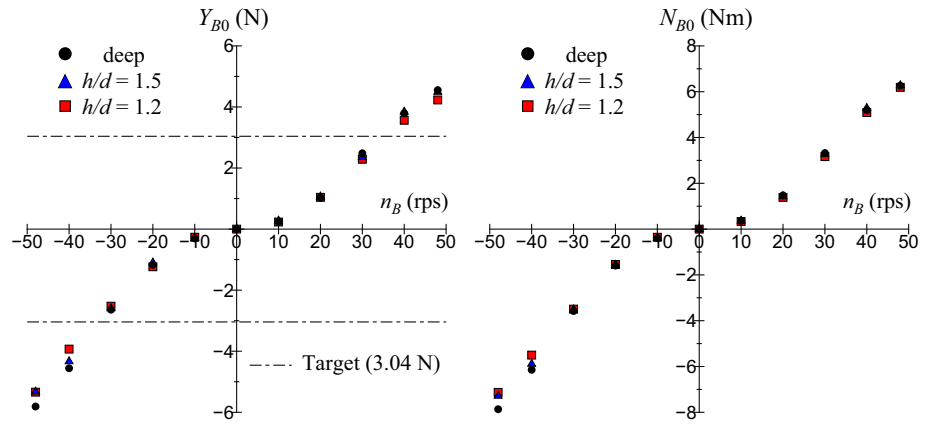

Fig. 22 f_X, f_Y, and f_N representing the forward speed effect on the hydrodynamic forces generated by BT in three different water depths

Table 6 K_{NB} in different water depths

h/d	Deep	1.5	1.2
$n_B > 0$	0.302	0.296	0.282
$n_B < 0$	0.327	0.323	0.309

no piers. The ship shadows in the graph were drawn at the ship positions every 10 s from the start of the movement. The calculated trajectory during the lateral movement to the port side agreed with the experiment with practical accuracy. The calculated trajectory to the starboard side was further forward than that of the experiment. Figure 24 shows the time history of the BT impeller revolution n_B between calculation and experiment. The calculated n_B approximately

agrees with the experimental values for $\delta = \pm 35°$. Thus, the proposed BT impeller control model is valid.

Figure 25 shows time histories of drift angle β, heading angle ψ, propeller thrust T, and rudder normal force F_N between calculation and experiment in deep water ($\delta = +35°$). The calculated β approached approximately 30° over time. However, the measured β remained constant at approximately 40°. The calculated ψ exhibited slight fluctuations during the initial lateral movement. However, the maximum fluctuation amplitude was smaller than 1°. As time passes, ψ converges to nearly zero. The proposed BT impeller revolution control model worked well for lateral motion simulations. However, ψ in the experiment fluctuated with a deviation of approximately 5°. The BT impeller in the experiment was adjusted, such that ψ was zero. However,

Fig. 23 Comparison of ship trajectories for lateral moving with $\delta = \pm 35°$ between calculation and experiment in deep water
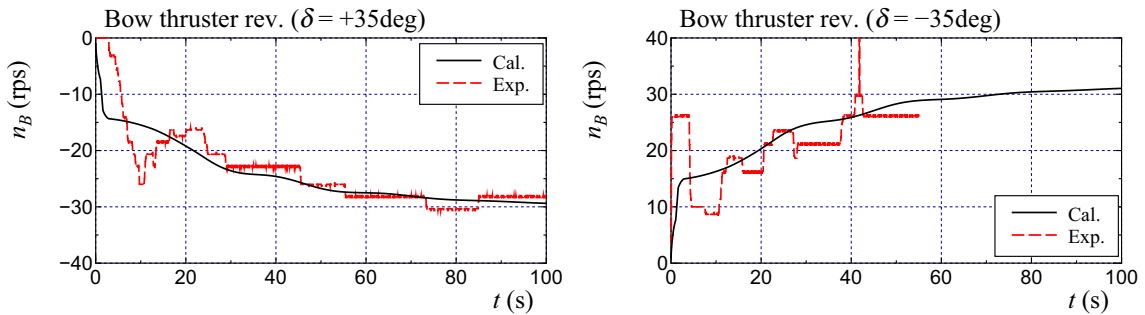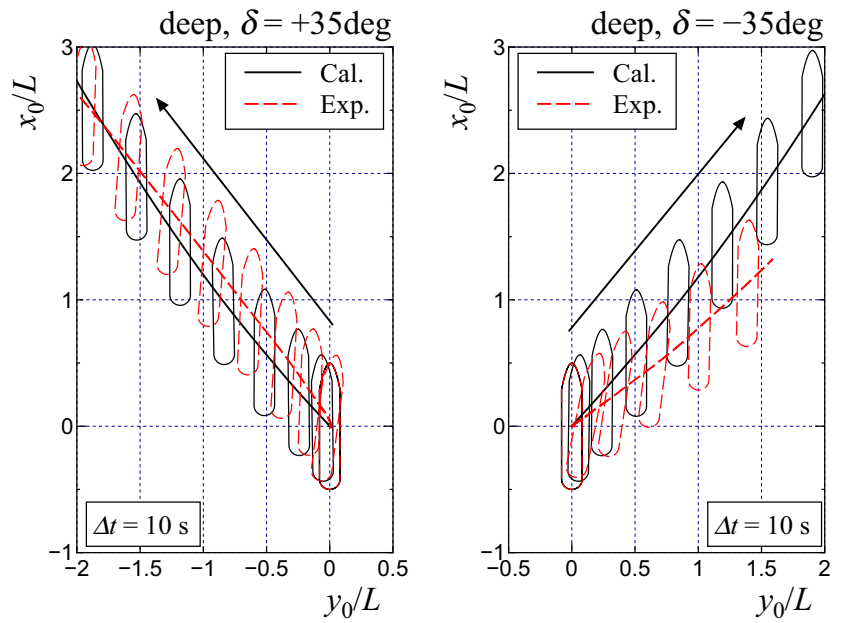

Fig. 24 Comparison of time histories of BT impeller revolution n_B between calculation and experiment in deep water
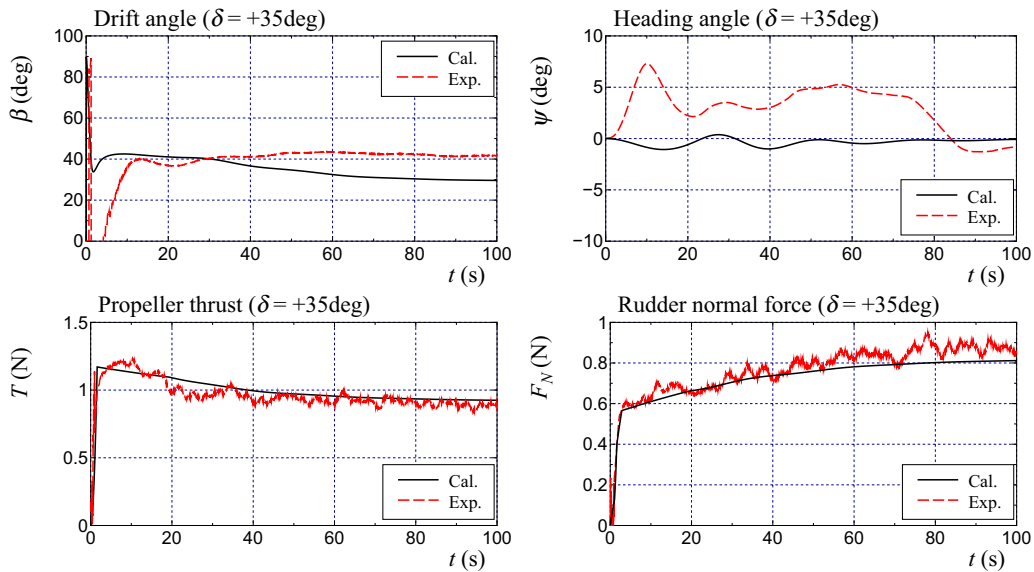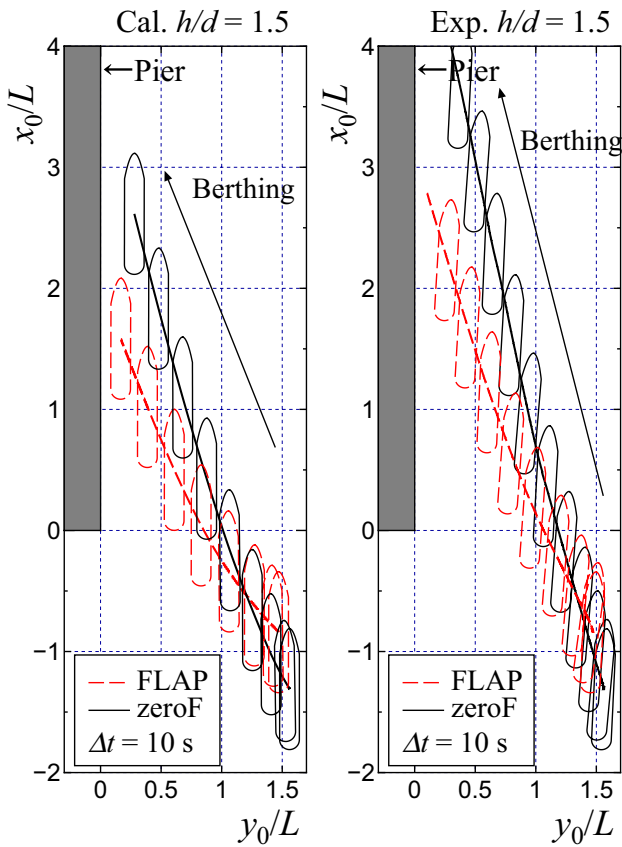

Fig. 25 Comparison of time histories of drift angle β, heading angle ψ, propeller thrust T, and rudder normal force F_N between calculation and experiment in deep water ($\delta = +35°$)

Fig. 26 Comparison of berthing trajectories between calculation and experiment for FLAP and zeroF conditions ($h/d = 1.5$)

water depth was $h/d = 1.5$, and the rudder angle was set to $\delta = +35°$. The ship was berthed on the port side of the pier, and the berthing maneuver was started from position $(x_0/L, y_0/L) = (-1.0, 1.5)$ in the simulations. The trajectory for zeroF moves forward compared to that for FLAP. This calculation can qualitatively capture the difference in trajectories between FLAP and zeroF. However, the calculations indicated less forward movement than the experiments. Figure 27 shows the time histories of the BT impeller revolution n_B for FLAP and zeroF conditions. The calculated n_B values agreed well with the experimental values for both FLAP and zeroF.

Figure 28 shows the comparison of time histories of β, ψ, T, and F_N for FLAP and zeroF conditions. The calculated β is larger than the experimental value at the initial stage of berthing for both FLAP and zeroF, and a difference can be observed. However, the calculated β approached the experimental value as time progressed. The calculated ψ is almost zero for both FLAP and zeroF, and the heading can be maintained as constant. However, a quantitative difference was observed between the calculated and measured ψ. This is owing to the poor performance of the heading control using BT in the experiment. The calculated T and F_N values agreed with the experimental results with practical accuracy for both FLAP and zeroF.

4.5 Berthing simulations in different water depths

Figure 29 shows the comparison of ship trajectories while berthing in $h/d = 1.5$ and 1.2. The rudder was a FLAP, and the rudder angle was set to $\delta = +35°$. For $h/d = 1.5$, the calculation approximately captured the berthing behavior in the experiment, although the forward movement was more suppressed than in the experiment. The ship model could not move laterally while approaching the pier in the experiment with $h/d = 1.2$ and turned. The calculations approximately captured this phenomenon. This is because the BT thrust, which was determined to balance the lateral force generated by the rudder, was too small to maintain a constant heading. Figure 30 shows the time history of the BT impeller
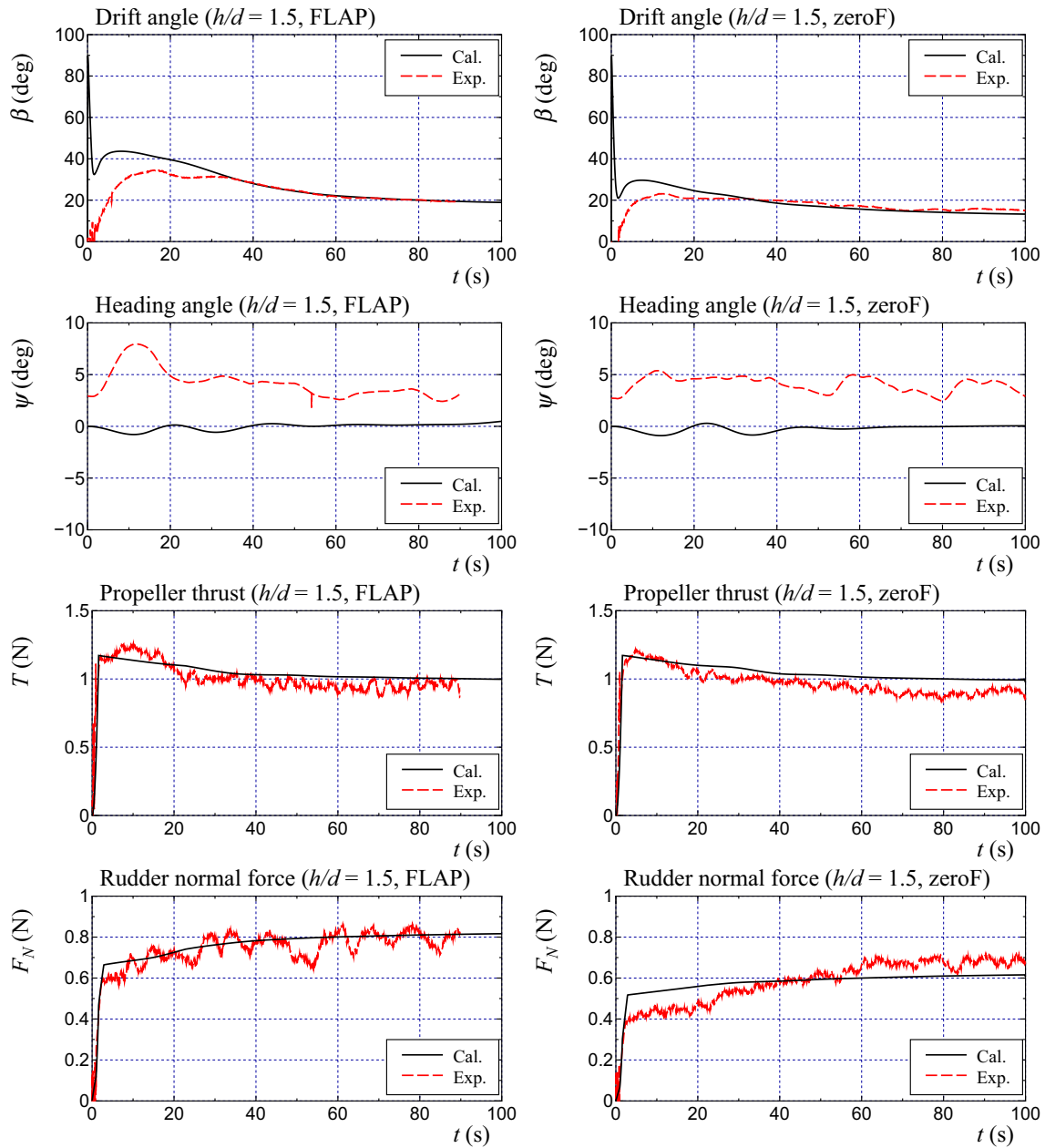
a certain amount of error was unavoidable, because it was manually controlled. The T and F_N in the calculations agree well with those in the experiments.

4.4 Berthing simulations for FLAP and zeroF

Figure 26 shows the comparison of ship trajectories while berthing using two rudders of the flapped rudder (FLAP) and the zero flapped rudder (zeroF). The

Fig. 27 Comparison of time histories of BT impeller revolutions n_B between calculation and experiment for FLAP and zeroF conditions ($h/d = 1.5$)

Fig. 28 Comparison of time histories of drift angle β, heading angle ψ, propeller thrust T, and rudder normal force F_N between calculation and experiment for FLAP and zeroF conditions

revolution n_B in $h/d = 1.5$ and 1.2. n_B at $h/d = 1.2$ becomes constant after $t = 40$s, indicating that a limiter is applied. To achieve berthing when $h/d = 1.2$, it is necessary to increase the capacity of the BT thrust or decrease the propeller revolution to reduce the rudder force generated. In the latter case, the lateral speed decreased. Note that the phenomenon in which the ship cannot move laterally is unrelated to the

presence of the pier, because the bank effect is not considered in the calculations.

Figure 31 shows comparison of the time histories of β, ψ, T, and F_N in $h/d = 1.5$ and 1.2. The calculated β was larger than the experimental value at the initial stage of berthing for both $h/d = 1.5$ and $h/d = 1.2$, although the calculated β approached the experimental value over time.
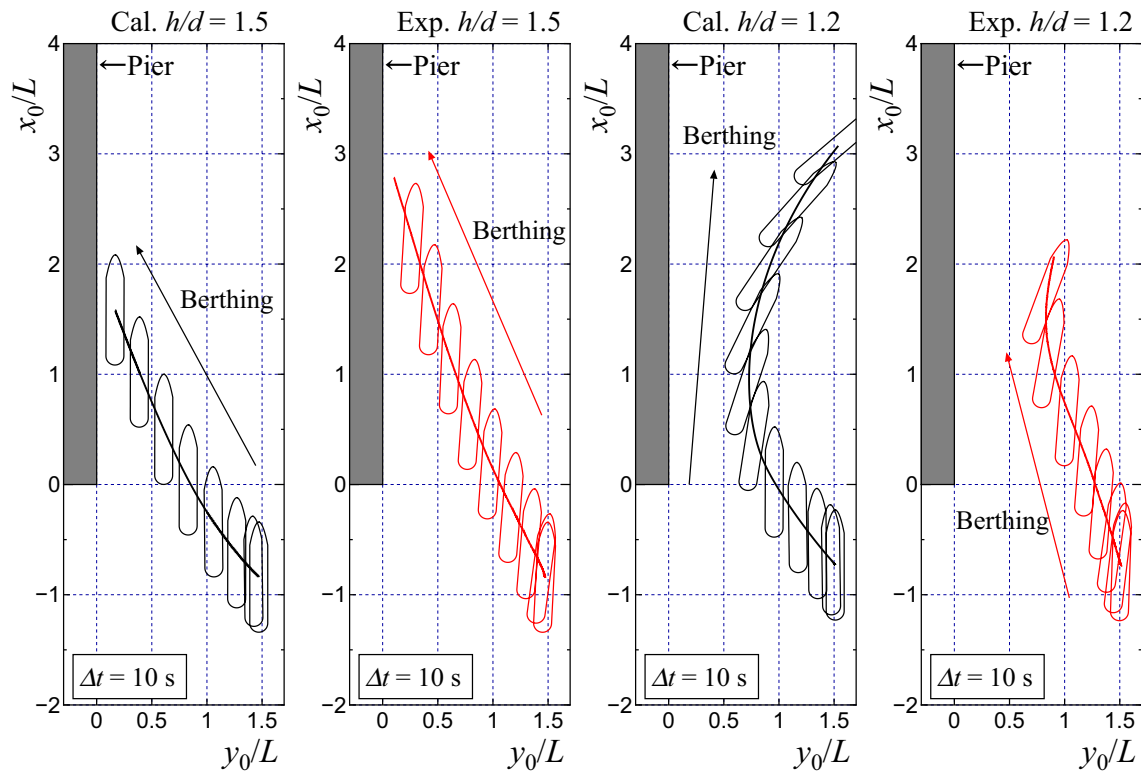
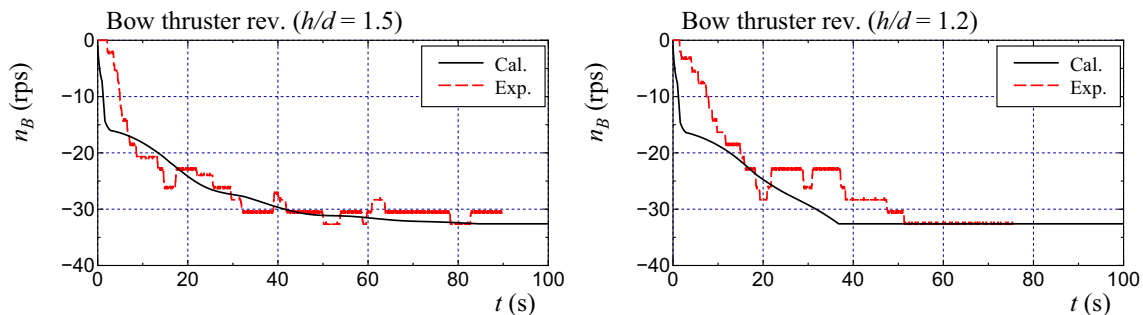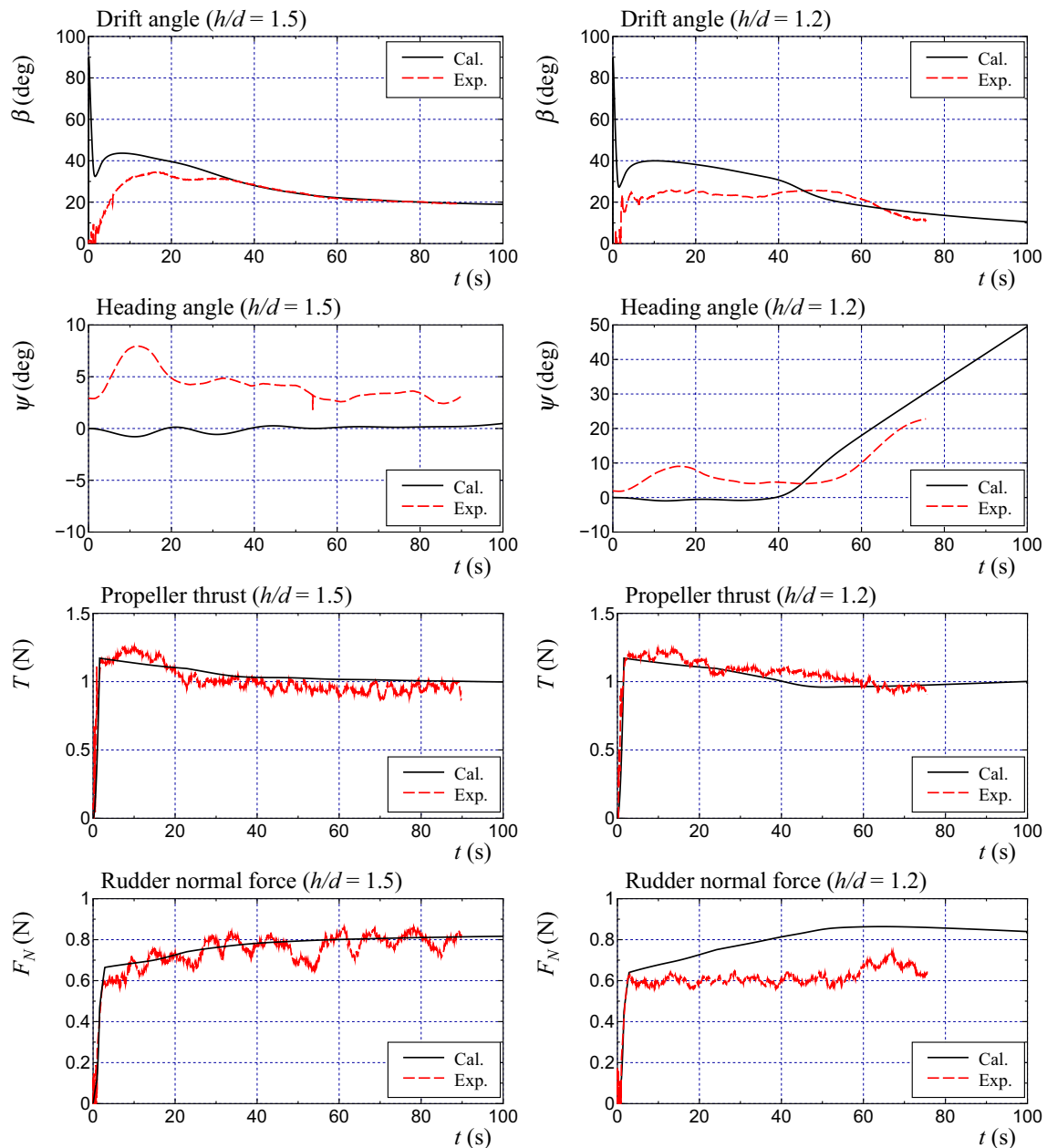**Fig. 29** Comparison of berthing trajectories between calculation and experiment in $h/d = 1.5$ and 1.2

Fig. 30 Comparison of time histories of BT impeller revolution n_B between calculation and experiment in $h/d = 1.5$ and 1.2

The calculated ψ was almost zero for $h/d = 1.5$. However, a quantitative difference was observed between the calculated and measured ψ. ψ in the experiment at $h/d = 1.2$ suddenly increased at approximately $t = 40$ s and began to turn. The calculated ψ exhibited similar behavior to that of the experiment. The calculated T values agree well with the experimental values at each water depth. The calculated F_N value agrees well with the experimental value for $h/d = 1.5$.

However, for $h/d = 1.2$, the calculated F_N was larger than that in the experiment.

In summary, the calculations approximately capture the experiments, although there is room for quantitative improvement in the ship trajectories.

Fig. 31 Comparison of time histories of drift angle β, heading angle ψ, propeller thrust T, and rudder normal force F_N between calculation and experiment in $h/d = 1.5$ and 1.2

5 Conclusion

In this study, the berthing and unberthing performance was investigated for a single-propeller and single-rudder inland container ship with a flapped rudder and bow thruster using free-running model tests. In the tests, a navigation method was employed in which the BT impeller revolution was manually adjusted to maintain the ship heading parallel to the pier ($\psi = 0°$) under a constant rudder angle and propeller revolution (OSN-method). The ship model sailed in oblique moving conditions during berthing and unberthing. The effects of a flapped rudder, the magnitude of the rudder angle, and water depth on the berthing and unberthing

performance were investigated using free-running model tests. In addition, lateral movement or berthing calculations were conducted using the low-speed maneuvering model presented by Okuda et al. [8] incorporating a BT impeller controller to simulate the OSN-method. The calculation results were compared with free-running model test results for validation. The findings of this study are as follows:

- The proposed navigation method (OSN-method) makes the ship possible to berth and unberth in the shallow water of $h/d = 1.5$, although the ship gradually moves forward. The free-running test using the OSN-method is useful for evaluating the berthing and unberthing performance of single-shaft ships with a bow thruster. In the case of the present ship, the optimum rudder angle for lateral moving was $\pm 35°$ when using a flapped rudder. The use of a normal rudder deteriorates the berthing and unberthing performance. When the water depth becomes shallow, such as $h/d = 1.2$, it becomes difficult for the ship to berth and unberth.
- The low-speed maneuvering simulation model incorporating the BT impeller controller for lateral moving can simulate the berthing motion with practical accuracy. However, as the water depth becomes shallow, the calculation accuracy of the ship trajectory deteriorates. This should be improved.

To improve calculation accuracy, it is necessary to consider the bank effect on the hydrodynamic forces acting on the ship during berthing and unberthing. We intend to conduct further studies to improve the proposed model.

References

1. Kose K, Fukuto J, Sugano K, Akagi S, Harada M (1986) On a computer aided maneuvering system in harbours. J Soc Naval Archit Japan 160:103–110 (**in Japanese**)
2. Koyama T, Yan J, Huan JK (1987) A systematic study on automatic berthing control (1st report). J Soc Naval Archit Japan 162:201–210 (**in Japanese**)
3. Yamato H, Koyama T, Nakagawa T (1993) Automatic berthing system using expert system. J Soc Naval Archit Japan 174:327–337 (**in Japanese**)
4. Wu G, Zhao X, Wang L (2021) Modeling and simulation of automatic berthing based on bow and stern thruster assist for unmanned surface vehicle. J Mar Sci 3(2):16–21
5. Hasegawa K, Kitera K (1993) Automatic berthing control system using network and knowledge base. J Kansai Soc Naval Archit 220:135–143 (**in Japanese**)
6. Maki A, Sakamoto N, Akimoto Y, Nishikawa H, Umeda N (2020) Application of optimal control theory based on the evolution strategy (CMA-ES) to automatic berthing. J Mar Sci Technol 25:221–233
7. Sawada R, Hirata K, Kitagawa Y, Saito E, Ueno M, Tanizawa K, Fukuto J (2021) Path following algorithm application to automatic berthing control. J Mar Sci Technol 26:541–554
8. Okuda R, Yasukawa H, Yamashita T, Matsuda A (2023) Maneuvering simulations at large drift angles of a ship with a flapped rudder. Appl Ocean Res 135:103567
9. Suzaku, http://www.ikous.co.jp/suzaku/index.html (in Japanese)
10. Furukawa T, Umeda N, Matsuda A, Terada D, Hashimoto H, Stern F, Araki M, Sadat-Hosseini H (2012) Effect of hull form above calm water plane on extreme ship motions in stern quartering waves. In: Proc. 29th Symp. on Naval Hydrodynamics, Gothenburg, Sweden, 1–11
11. Matsuda A, Hashimoto H, Terada D, Taniguchi Y (2016) Validation of free running model experiments in heavy seas. In: Proc. 3rd International Conference on Violent Flows, Osaka, Japan
12. Hasnan MAA, Yasukawa H, Hirata N, Terada D, Matsuda A (2020) Study of ship turning in irregular waves. J Mar Sci Technol 25(4):1024–1043
13. Yasukawa H, Yoshimura Y (2015) Introduction of MMG standard method for ship maneuvering predictions. J Mar Sci Technol 20(1):37–52
14. Yasukawa H, Kawamura S, Tanaka S, Sano M (2009) Evaluation of ship-bank and ship-ship interaction force using a 3D panel method. In: Int. Conf. on Ship Manoeuvring in Shallow Water and Confined Water, Antwerp, Belgium, pp 127–133
15. Yoshimura Y, Sakurai H (1989) Mathematical model for the manoeuvring ship motion in shallow water (3rd report)—manoeuvrability of a twin-propeller twin rudder ship. J Kansai Soc Naval Archit 211:115–126 (**in Japanese**)